Valence Contrast between Iron Sites in α-Fe_2PO_5: A Comparative Study by Magnetic Neutron and Resonant X-ray Powder Diffraction

Joanne K. Warner,[†] Anthony K. Cheetham,*[†,‡] David E. Cox,[§] and Robert B. Von Dreele[∥]

Contribution from the Chemical Crystallography Laboratory, University of Oxford, 9 Parks Road, Oxford OX1 3PD, U.K., Brookhaven National Laboratory, Upton, Long Island, New York 11973, and LANSCE, Los Alamos National Laboratory, Los Alamos, New Mexico 87545. *Received October 15, 1991*

Abstract: α-Fe_2PO_5 is a mixed valence compound (space group *Pnma*, a = 7.3639 (7) Å, b = 6.4320 (6) Å, c = 7.4550 (7) Å, Z = 4, V = 353.1 (1) Å^3) in which Fe^{2+} and Fe^{3+} are apparently located in two different crystallographic sites. The distribution of these two species within the structure has been investigated by Rietveld analysis of both magnetic neutron and resonant X-ray powder diffraction data, and the results have been compared with bond valence calculations. At energies close to the Fe^{2+} K-edge determined from XANES, the M(1) site possesses a more negative value of f' (f'(M(1)) = −9.74 (5), f'(M(2)) = −8.04 (7)), whereas at energies near the Fe^{3+} edge, M(2) shows the most negative f' value (f'(M(1)) = −6.75 (11), f'(M(2)) = −10.01 (17)). α-Fe_2PO_5 orders antiferromagnetically at temperatures below 250 K, and neutron diffraction is used to solve the magnetic structure and refine values for the magnetic moment at each iron site (M(1) = 3.89 (3) μ_B, M(2) = 4.22 (3) μ_B). Both diffraction experiments are consistent with the presence of Fe^{2+} at M(1) and Fe^{3+} at M(2) and are in agreement with bond valence calculations ($\sum s_{M(1)}$ = 2.077 (3), $\sum s_{M(2)}$ = 2.997 (7)) based upon the room-temperature crystal structure.

Introduction

The determination of valence distributions in solid-state materials is of considerable interest to chemists, biologists, physicists, and mineralogists. The mixed valent compounds of iron form the largest group known for any element and comprise oxides, hydroxides, halides, sulfates, cyanides, phosphates, carbonates, acetates, silicates, borates, and sulfites.[1] A recent review of iron phosphates and oxyphosphates[2] highlights the enormous scope within this system alone, with unusual magnetic properties resulting from the interplay between structure and valence. These materials generally display antiferromagnetic transitions, although weak ferrimagnetism, frustration, and spin canting have also been observed.[3-7]

Fe_2PO_5 has two polymorphs, the low-temperature tetragonal β-phase (space group = $I4_1/amd$, a = 5.3360 (7) Å, c = 12.457 (2) Å, Z = 4, V = 354.7 (1) Å^3) having only one crystallographic site for iron (average valence 2.5) within continuous chains of face-sharing FeO_6 octahedra. Our earlier study of the magnetic structure of β-Fe_2PO_5 (T_N = 408 K) found that ferromagnetic exchange occurred between the cations within each chain by a Verwey double exchange mechanism, with antiferromagnetic interactions occurring between perpendicular chains.[8] At temperatures above 800 °C, an irreversible transition occurs from the β- to the α-phase (space group = *Pnma*, a = 7.3639 (7) Å, b = 6.4320 (6) Å, c = 7.4550 (7) Å, Z = 4, V = 353.1 (1) Å^3) with iron located in two different crystallographic sites of the orthorhombic cell. Mössbauer spectra of α-Fe_2PO_5 at temperatures from 90 to 873 K are consistent with electron localization of Fe^{2+} and Fe^{3+}, despite the short distance (2.92 Å) between the M(1) and M(2) sites.[9,10] Magnetic susceptibility measurements indicate that α-Fe_2PO_5 orders antiferromagnetically below T_N = 250 K.[9] The M(1) site is surrounded by an octahedral arrangement of oxygens, which form chains parallel to the b-axis and share edges. The octahedra containing the M(2) cations are connected to these chains by sharing faces with two M(1) O_6 octahedra, alternating sides with the phosphate tetrahedra (Figure 1).

Two types of diffraction experiments can directly confirm the valence of these individual iron sites. Magnetic neutron diffraction at temperatures below T_N can be used to determine the magnetic structure of the compound and, hence, the value of the moment at each site. Resonant X-ray powder diffraction at wavelengths in the vicinity of the Fe K-edge can exploit the slight differences in energy of the Fe^{2+} and Fe^{3+} absorption edges to detect a contrast in anomalous scattering power between the two sites.

The large range of X-ray wavelengths available at synchrotron sources enables us to utilize resonant scattering effects for any element that has an absorption edge at an accessible energy, typically 4–25 keV depending upon the diffraction optics. Resonant X-ray powder diffraction techniques have been successfully used to enhance the contrast in scattering between elements with similar atomic numbers[11-15] and, more recently, to distinguish between the different valence states of the resonant element.[16-19] The position and shape of an absorption edge are affected by both the valence and coordination environment of the element and are dependent upon the binding energy of the core electrons undergoing transitions to excited states. Studies of the relationship between effective atomic charge and chemical shifts in K ab-

[†] University of Oxford.
[‡] Present address: Materials Department, University of California, Santa Barbara, CA 93106.
[§] Brookhaven National Laboratory.
[∥] Los Alamos National Laboratory.

(1) Robin, M. B.; Day, P. *Adv. Inorg. Chem. Radiochem.* **1967**, *10*, 247.
(2) Gleitzer, C. *Eur. J. Solid State Inorg. Chem.* **1991**, *28*, 77.
(3) Beltran-Porter, D.; Olazcuaga, R.; Fournes, L.; Menil, F.; Le Flem, G. *Rev. Phys. Appl.* **1980**, *15*, 1155.
(4) Moya-Pizzaro, T.; Salmon, R.; Fournes, L.; Le Flem, G.; Wanklyn, B.; Hagenmuller, P. *J. Solid State Chem.* **1984**, *53*, 387.
(5) Battle, P. D.; Cheetham, A. K.; Gleitzer, C.; Harrison, W. T. A.; Long, G. L.; Longworth, G. *J. Phys. C: Solid State Phys.* **1982**, *15*, L919.
(6) Modaressi, A.; Courtois, A.; Geradin, R.; Gleitzer, C. *J. Solid State Chem.* **1983**, *47*, 245.
(7) Warner, J. K.; Cheetham, A. K.; Nord, A. G.; Von Dreele, R. B.; Yethiraj, M. *J. Mater. Chem.* **1992**, *2*, 191.
(8) Ijjaali, M.; Malaman, B.; Gleitzer, C.; Warner, J. K.; Hriljac, J. A.; Cheetham, A. K. *J. Solid State Chem.* **1990**, *86*, 195.
(9) Modaressi, A.; Courtois, A.; Geradin, R.; Malaman, B.; Gleitzer, C. *J. Solid State Chem.* **1981**, *40*, 301.
(10) Iraldi, R.; Le Caer, G.; Gleitzer, C. *Solid State Commun.* **1981**, *40*, 145.
(11) Perkins, D. A.; Attfield, J. P. *J. Chem. Soc., Chem. Commun.* **1991**, *4*, 229.
(12) Warner, J. K.; Wilkinson, A. P.; Cheetham, A. K.; Cox, D. E. *J. Phys. Chem. Solids* **1991**, *52*, 1251.
(13) Yakel, H. L. *Acta Crystallogr.* **1983**, *B39*, 20.
(14) Moroney, L. M.; Thompson, P.; Cox, D. E. *J. Appl. Crystallogr.* **1988**, *21*, 206.
(15) Duncan, J. F.; Freeman, A. G.; Johnston, J. H. *Anomalous Scattering*; Ramaseshan, S., Abrahams, S. C., Eds.; Munksgaard: Copenhagen, 1974; p 163.
(16) Attfield, J. P. *Nature* **1990**, *343*, 46.
(17) Kwei, G. H.; Von Dreele, R. B.; Williams, A.; Goldstone, J. A.; Lawson, A. C., II; Warburton, W. K. *J. Mol. Struct.* **1990**, *223*, 383.
(18) Wilkinson, A. P.; Cheetham, A. K.; Cox, D. E. *Acta Crystallogr.* **1991**, *B47*, 155.
(19) Attfield, J. P. *J. Phys. Chem. Solids* **1991**, *52*, 1243.

0002-7863/92/1514-6074$03.00/0

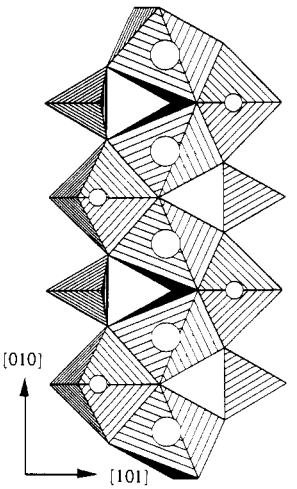

Figure 1. Chains of face-sharing FeO_6 octahedra and PO_4 tetrahedra running parallel to the *b*-axis in α-Fe_2PO_5. The M(1) sites are depicted by larger circles than the M(2) sites.

sorption spectra of transition metal compounds indicate that the energy of the edge position increases 2–6 eV for each unit increase in oxidation number.[20,21] The value for the atomic scattering factor, f ($f = f_o + f' + if''$), changes rapidly in the region of the absorption edge as the real (f') and imaginary (f'') components of the anomalous scattering fluctuate. Even a 3 eV energy difference between the edge positions of two different oxidation states of the same element can lead to measurable differences in their scattering power at wavelengths close to the edge. Absorption by the resonant element is related to f'' via the optical theorem,[22] and measurements show that it increases sharply in the edge region, reaching a maximum several electronvolts above the f' minimum. Ideally, energies a few electronvolts below the absorption edge are chosen for diffraction experiments, where the values of f' are large and negative, and values of f'', and hence absorption and fluorescence, are low. In this study, the position of the Fe^{2+} K-edge in α-Fe_2PO_5 was measured by XANES spectroscopy; diffraction patterns were then collected in the region of the Fe^{2+} and Fe^{3+} absorption edges and also at a much lower energy where differences in f' for Fe^{2+} and Fe^{3+} were predicted to be minimal.

In contrast with this innovative X-ray technique, the magnetic moment of a neutron has been used to explore the magnetic structure of crystalline materials for many years.[23,24] The first detection of antiferromagnetism by neutron diffraction was reported by Shull and Smart in 1949.[25] Combined with the ability to determine the magnetic moment associated with each iron site in our compound at temperatures below T_N, neutron diffraction offers greater precision for the determination of light element positions and temperature factors. However, its general use for the determination of valence is limited to species which possess a magnetic moment, and the magnetic structure of some compounds may be too complex for powder data to yield conclusive results.

Experimental Section

The sample was prepared by dissolving stoichiometric amounts of $Fe(NO_3)_3{\cdot}9H_2O$ and $NH_4H_2PO_4$ in distilled water and evaporating to dryness. The nitrate mixture was decomposed at 300 °C, and pellets were sintered at 850 °C for 5 days under vacuum in a silica tube with regular regrinding. X-ray powder diffraction was used to check sample purity. Samples prepared at higher temperatures were found to exhibit severe preferred orientation. Analytical electron microscopy[26] of the final product showed the P:Fe ratio to be 1:2.01 (3).

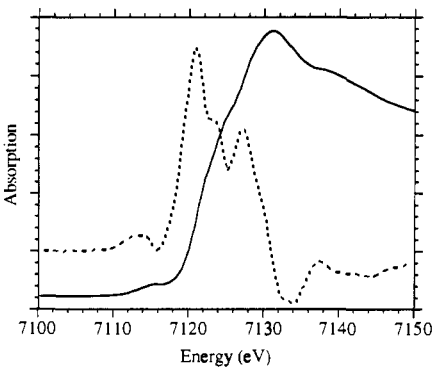

Figure 2. XANES absorption spectrum of α-Fe_2PO_5 measured in the region of the Fe K-edge. The first differential (---) is superimposed over the spectra to show the energy of the first maximum, denoted as the Fe^{2+} absorption edge in our discussions.

XANES spectra at the Fe K-edge of α-Fe_2PO_5 were collected on station 7.1 at the Synchrotron Radiation Source (SRS), Daresbury Laboratory. Approximately 50 mg of sample was mixed with boron nitride as a diluent and mounted between cellulose tape in the window of an aluminum sample holder. The monochromator was scanned across the Fe K-edges over an energy range of 7044.8–7261.8 eV with an estimated band pass of around 2 eV. The energy calibration was determined by measuring the absorption edge of an iron foil (7112.0 eV[27]). Figure 2 shows the absorption spectrum of α-Fe_2PO_5, with the low-energy maxima in the derivative assigned to the Fe^{2+} edge at 7120.9 (4) eV. Although the energy of the Fe^{3+} edge is less well defined and could be at either of the observed features at 7123 and 7127 eV, the former seems more likely. We have observed typical chemical shifts of 2–4 eV between di- and trivalent iron oxides and phosphates.[28]

Synchrotron X-ray diffraction data below, and close to, the Fe^{2+} K-edge were collected from a flat plate sample using diffractometer 8.3 at the SRS. A channel cut Ge(111) crystal monochromator was used to select the wavelength, with a beam-defining vertical slit of 2 mm giving a band pass of around 3.0 eV at the sample position. With the detector $\theta/2\theta$ set to a region devoid of peaks, the monochromator angle was varied to scan the energy range of interest with the fluorescence measured by the scintillation detector providing an estimate of the edge position and shape. The wavelength could then be selected accurately on the basis of these fluorescence measurements. Diffraction data close to the Fe^{3+} edge were collected on diffractometer 9.1, exploiting the extra intensity available from the 5-T wiggler source to work in this highly absorbing regime. A Si(111) channel cut monochromator and 0.5 mm vertical slits were used to reduce the band pass to 1.6 eV, and an intrinsic Ge solid-state detector (resolution FWHM 165 eV) was used to discriminate the Fe Kα fluorescence. In each experiment, the sample surface was slightly roughened in an attempt to reduce preferred orientation, and the flat plate sample holder was rotated to average the crystallite orientations. Data were collected from 18 to 110° 2θ with a step size of 0.01° for counting times of 2–3 s per point. All of the diffraction data were normalized to the incident monitor counts and scaled to counts s^{-1} 100 mA^{-1} ring current. An NBS silicon standard was used to calibrate the wavelength and zero point of the lowest energy data set, and the unit cell obtained from α-Fe_2PO_5 at this energy was used to calculate the wavelength of the subsequent experiments.

Time-of-flight neutron powder diffraction data were collected from a 5 g sample on the high-intensity powder diffractometer, HIPD, at LANSCE, Los Alamos. Data from the 153°, 90°, and 40° detector banks were used in the analysis, covering a range of *d* spacings from 0.4 to 9 Å. The sample was mounted in a $^1/_2$ in. diameter vanadium can and cooled by a Displex closed-cycle refrigerator. Data were collected at 12.1 (1) K and above the magnetic transition (T_N = 250 K) at 300 (1) K for around 2 h in each case.

Results and Discussion

1. Resonant X-ray Diffraction. The Rietveld[29] profile refinement program GSAS[30] was used to refine a single structural model using all of the X-ray data sets, while allowing the scale,

(20) Sarode, P. R.; Ramasesha, S.; Madhusudan, W. H.; Rao, C. N. R. *J. Phys. C: Solid State Phys.* **1979**, *12*, 2439.
(21) Wong, J.; Lytle, F. W.; Messmer, R. P.; Maylotte, D. H. *Phys. Rev. B* **1984**, *30*, 5596.
(22) James, R. W. *The Optical Principles of the Diffraction of X-rays*; Bell: London, 1948; p 135.
(23) Bloch, F. *Phys. Rev.* **1936**, *50*, 259.
(24) Halpern, O.; Johnson, M. H. *Phys. Rev.* **1939**, *55*, 898.
(25) Schull, C. G.; Smart, J. S. *Phys. Rev.* **1949**, *76*, 1256.
(26) Cheetham, A. K.; Skarnulis, A. J. *Anal. Chem.* **1981**, *53*, 1060.
(27) Bearden, J. A.; Burr, A. F. *Rev. Mod. Phys.* **1967**, *39*, 125.
(28) Warner, J. K.; Cheetham, A. K. Unpublished results.
(29) Rietveld, H. M. *J. Appl. Crystallogr.* **1969**, *2*, 65.
(30) Larson, A. C.; Von Dreele, R. B. Los Alamos National Laboratory Report No. LA-UR-86-748, 1987.

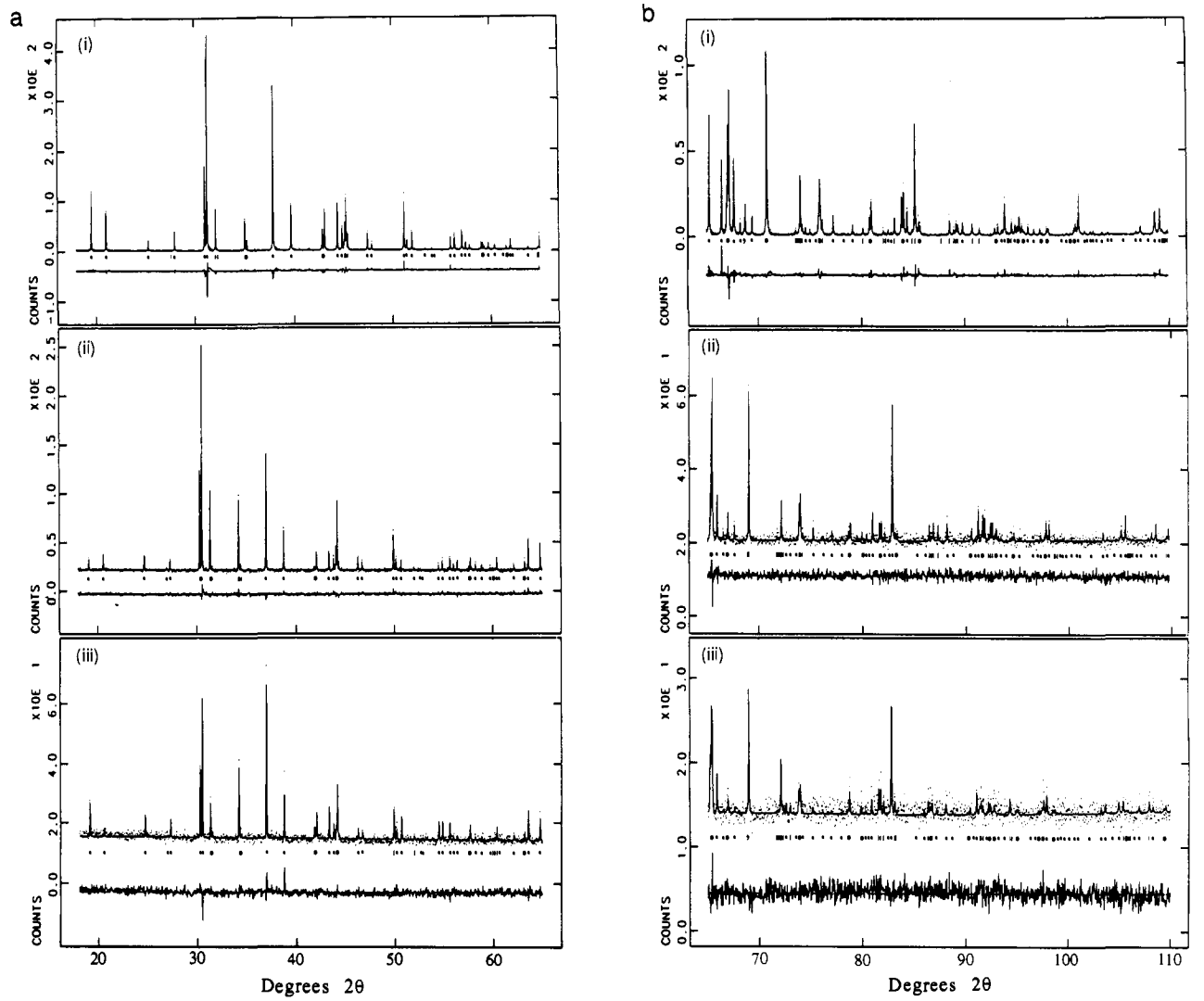

Figure 3. Observed (dots), calculated (solid line), and difference profiles of room-temperature synchrotron X-ray data at wavelengths (i) 1.783 16 (1) Å, (ii) 1.741 79 (2) Å, and (iii) 1.740 18 (6) Å. The data sets have been split into (a) low and (b) high angle regions to give appropriate scales. The reflection positions are shown by marker bars.

background, peak shape, and f' for each iron site to vary for each data set. Significant preferred orientation was observed, and the best results were obtained when a component along the [123] direction was refined. A "pseudo-Voigt" peak shape with a correction for low angle asymmetry and a three-term cosine Fourier series background function were used. The polarization ratio was assigned the estimated value of 0.94. Because of the relatively small range of sin θ/λ (0.09–0.47) covered at these wavelengths, the temperature factors and f' values were found to be highly correlated. The former were therefore fixed at the isotropic values obtained from the 300 K neutron study. Free neutral atom scattering factors were used for all elements, with starting f' values calculated at each wavelength using the program FPRIME.[31] The values of f' for the two iron sites were initially constrained to be the same until the refinement neared convergence, after which time they were allowed to refine independently. The resulting f' values are given in Table I with the observed and calculated profiles shown in Figure 3. R factors, as defined in ref 29, and structural parameters are given in Tables II and III, respectively. Attempts to refine f'' were inconclusive, and these were accordingly fixed at values estimated from comparable positions at the Fe metal edge determined by interferometry.[32] The lowest energy values were calculated using FPRIME.[31] The effect of changing f'' from 0.4 to 4 electrons did not change the values of f' by more than 0.2 electron.

(31) Cromer, D. T. *J. Appl. Crystallogr.* **1983**, *16*, 437.
(32) Begum, R.; Hart, M.; Lea, K. R.; Siddons, D. P. *Acta Crystallogr.* **1986**, *A42*, 456.

Table I. Refined Values of f' Obtained for the M(1) and M(2) Sites in α-Fe_2PO_5

	diffractometer		
	8.3	8.3	9.1
wavelength (Å)	1.783 16 (4)	1.741 79 (1)	1.740 18 (6)
energy (eV)	6953.1 (1)	7118.3 (1)	7124.8 (3)
ΔE from Fe^{2+} K-edge (eV)	−165.2 (5)	−2.6 (5)	3.9 (5)
estimated band pass (eV)	3.0 (2)	3.0 (2)	1.6 (2)
f' (M(1)) (electrons)	−3.57 (4)	−9.74 (5)	−6.75 (11)
f' (M(2)) (electrons)	−3.56 (5)	−8.04 (7)	−10.01 (17)
f'' (M(1)) (electrons)	0.472	1.8	4.0
f'' (M(2)) (electrons)	0.472	1.7	3.2

The similarity between the refined f' values for M(1) and M(2) in the off-edge position at 6953.1 (1) eV and the high precision obtained indicate the sensitivity of the powder diffraction results to the scattering power of the two iron sites. The differences observed between the values of f' in the edge region show clearly that the magnitude of the real part of the anomalous scattering correction is greatest for M(1) near the Fe^{2+} edge and for M(2) near the Fe^{3+} edge. Comparison between the Cromer and Liberman free atom values of f' for iron and those from this experiment is shown in Figure 4. The theoretical curve has been shifted in energy to match the f' minima of Fe^{2+} and Fe^{3+} estimated from XANES. Although in qualitative agreement, the fit to the theoretical data is quite poor. This is not surprising as the theory does not take into account EXAFS, instrumental characteristics, or chemical bonding effects which influence the

Table II. Details of Simultaneous Rietveld Refinements

	no. data	no. refln	wR_p (%)	R_p (%)	R_{Exp} (%)	R_{Nuc} (%)	R_{Mag} (%)
A. X-ray Data at 300 (1) K							
diffractometer							
8.3	9499	170	20.76	14.72	10.81	8.96	
8.3	9499	170	4.13	3.27	3.54	14.21	
9.1	9199	170	5.63	4.47	4.15	28.03	
χ^2 = 2.30 for 52 variables							
a = 7.3730 (2) Å, b = 6.4404 (2) Å, c = 7.4652 (2) Å, V = 354.48 (2) Å^3							
B. Time-of-Flight Neutron Powder Data[a] at 300 (1) K							
detector							
153°	4547	1802	5.77	3.74	5.02	3.56	
90°	5528	1775	5.11	3.34	4.50	2.89	
40°	4310	233	5.48	3.80	4.51	3.81	
χ^2 = 1.36 for 53 variables							
a = 7.3639 (7) Å, b = 6.4320 (6) Å, c = 7.4550 (7) Å, V = 353.10 (10) Å^3							
C. Time-of-Flight Neutron Powder Data[a] at 12.1 (1) K							
detector							
153°	4545	2618	5.63	3.66	4.88	2.41	8.43
90°	5225	2617	5.22	3.60	4.38	4.00	3.25
40°	5252	1079	5.83	3.93	4.83	5.05	4.68
χ^2 = 1.41 for 52 variables							
a = 7.3881 (3) Å, b = 6.4142 (2) Å, c = 7.4179 (3) Å, V = 351.53 (4) Å^3							

[a] The time-of-flight neutron powder data were collected at the 153°, 90°, and 40° detector banks on HIPD.

Table III. Structural Parameters for α-Fe_2PO_5 Obtained by Rietveld Refinement Using (a) Three X-ray Powder Diffraction Data Sets[a] at Room Temperature, (b) 300 K, and (c) 12.1 K Time-of-Flight Neutron Powder Data[b]

atom		x	y	z	U_{iso} × 100 (Å^2)
M(1)	a	0	0	0	0.38
	b	0	0	0	0.38 (2)
	c	0	0	0	0.06 (1)
M(2)	a	0.3442 (2)	0.75	0.2132 (2)	0.15
	b	0.3443 (2)	0.75	0.2126 (2)	0.15 (2)
	c	0.3409 (1)	0.75	0.2133 (1)	0.02 (2)
P	a	0.3786 (2)	0.25	0.1295 (2)	0.47
	b	0.3787 (3)	0.25	0.1300 (3)	0.47 (3)
	c	0.3791 (3)	0.25	0.1295 (3)	0.25 (3)
O(1)	a	0.0978 (5)	0.75	0.1413 (5)	0.15
	b	0.0965 (3)	0.75	0.1422 (3)	0.15 (4)
	c	0.0971 (2)	0.75	0.1408 (2)	0.04 (3)
O(2)	a	0.7918 (5)	0.75	−0.0046 (4)	0.52
	b	0.7901 (3)	0.75	−0.0042 (3)	0.52 (4)
	c	0.7899 (2)	0.75	−0.0017 (3)	0.30 (3)
O(3)	a	0.0532 (5)	0.25	0.4791 (4)	0.78
	b	0.0533 (2)	0.25	0.4779 (3)	0.78 (5)
	c	0.0518 (2)	0.25	0.4784 (2)	0.28 (4)
O(4)	a	0.8691 (3)	0.4416 (3)	0.2484 (3)	0.36
	b	0.8679 (2)	0.4410 (2)	0.2471 (2)	0.36 (3)
	c	0.8675 (1)	0.4416 (1)	0.2473 (2)	0.06 (2)

[a] Two of these data sets were in the vicinity of the Fe K-edge. [b] The temperature factors for the X-ray study were fixed at the values obtained from the neutron data at the same temperature.

near-edge fine structure. The measured values of f' are affected by the energy range of the incident radiation, since band passes greater than the natural width of the absorption edge (1.25 eV for Fe K-edge[33]) broaden the shape of the intrinsic f' curve. This effect will be greatest in the 8.3 data set due to the poor energy resolution offered by the Ge(111) monochromator compared with Si(111) as a consequence of their differing Darwin widths. The true shapes of the Fe^{2+} and Fe^{3+} curves can only be determined using a larger number of data sets collected at energies through the edge and are expected to vary slightly in shape as a result of the differing chemical environments of M(1) and M(2).

The structural agreement, indicated by R_{Nuc}, highlights the dramatic deterioration in the quality of data as energies close to the absorption edge are encountered. It is interesting to note the inverse relationship between R_{Nuc} and the weighted profile R factor (wR_p) as a result of the high background levels.[34] Data collected

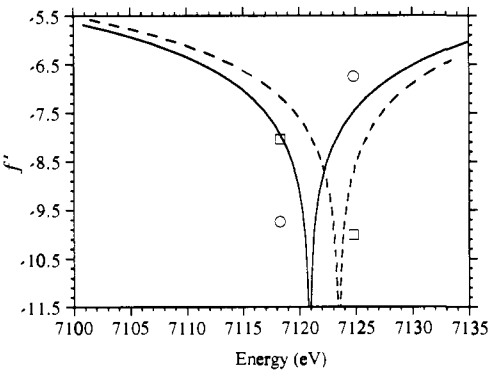

Figure 4. Cromer and Liberman free atom values of f' for iron, displaced in energy to the positions of the Fe^{2+} (—) and Fe^{3+} (- - -) absorption edges estimated from XANES. The values measured for the M(1) and M(2) sites at energies close to the edge are shown as larger diamonds and squares, respectively.

at an energy of 7135 eV, well above both the Fe^{2+} and Fe^{3+} absorption edges, on 9.1 had to be discarded from the refinement as severe absorption resulted in insufficient sampling of crystallites to maintain the powder average. An improved experimental strategy would be to collect a data set at a much shorter wavelength (say 0.8–1.2 Å) in order to cover a greater range in sin θ/λ and thereby obtain a better structural model, including temperature factors. Another data set, a few electronvolts below the first absorption edge, should be sufficient to distinguish between the scattering powers of the resonant sites without losing too much intensity to absorption processes.

2. Neutron Powder Diffraction. Nuclear and magnetic structure refinements were also performed with GSAS, as modified for magnetic refinements by M. Yethiraj. The nuclear structure of α-Fe_2PO_5 was refined using the 300 K neutron data set, and these parameters were used as the basis for the 12.1 K structure refinement. To avoid excessive correlation between the refined magnetic moment and the absorption correction, the values for the absorption correction obtained from the 300 K data were held constant in the 12.1 K refinement. We used the neutron scattering lengths from Koster and Yelon[35] and calculated the magnetic form

(33) Krause, M. O.; Oliver, J. H. *J. Phys. Chem. Ref. Data* **1979**, *8*, 329.

(34) Jansen, E.; Schafer, W.; Will, G. Poster presented at the International Workshop on the Reitveld Method, 13–15 June, 1989, Petten, The Netherlands.

(35) Koster, L.; Yelon, W. B. *Summary of Low Energy Neutron Scattering Lengths and Cross-Sections*; Netherlands Energy Research Foundation, Department of Physics: Petten, The Netherlands, 1982.

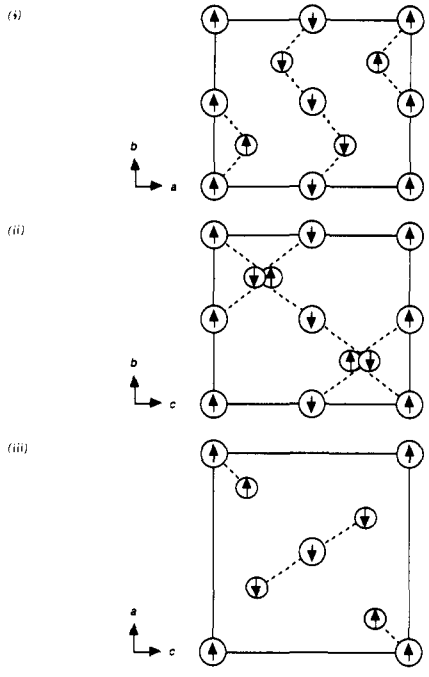

Figure 5. Final refined magnetic structure of α-Fe_2PO_5. For clarity, only the Fe^{2+} (large circles) and Fe^{3+} (small circles) have been shown.

factor for Fe^{2+} from the radial wave function using the Cambridge Crystallographic Subroutine Library.[36,37]

In the low-temperature profile, additional peaks of magnetic origin appeared which could be indexed on the same cell as the nuclear structure. The two strongest, purely magnetic, reflections were the (100) and (001), with the (101) and (201) nuclear reflections also gaining considerable magnetic intensity. Possible magnetic structures consistent with *Pnma* symmetry have been discussed extensively in the past.[38] From qualitative consideration of the magnetic intensities, the choices were narrowed down to the two collinear antiferromagnetic models involving either antiferromagnetic ordering within the chains of face-sharing octahedra or ferromagnetic ordering within the chains and antiferromagnetic ordering between them. These models were tested with a variety of collinear spin directions, with directions parallel to the *b*-axis being preferred by both. The second model produced significantly better magnetic *R* factors for each detector bank with an average value of 5.54% (compared with an average of 14.3% for the first) and was used in the refinement. The corresponding magnetic symmetry is *Pnma*. The final magnetic structure is shown in Figure 5. The values of the magnetic moments of M(1) and M(2) were allowed to refine independently, yielding 3.89 (3) μ_B and 4.22 (3) μ_B, compared with the refined value of the single $Fe^{2.5+}$ site in the β-phase (4.17 (3) μ_B[8]). We would expect the moment of Fe^{2+} (d^6) to be less than that of Fe^{3+} (d^5), although the value for Fe^{3+} is a little lower than expected (4.53 μ_B in $FePO_4$[5]) possibly due to covalency. Final *R* factors and structural parameters are given in Tables II and III, respectively.

The most probable magnetic exchange pathways (Figure 6) in the α-phase will be discussed, on the basis of the assumption that the M(1) site is occupied by Fe^{2+} and M(2) by Fe^{3+}, to ascertain their relative strengths and thus the structure-directing mechanism at 12 K.

(i) Direct Cation–Cation Interactions. Both types of FeO_6 octahedra share two of their faces with the other: the M(1) octahedron shares its opposite faces and the M(2) octahedron shares the adjoining faces either side of the basal plane. Under these conditions, the partially filled t_{2g} d orbitals are stabilized by the trigonal field produced by the oxygens and may provide sufficient orbital overlap to allow direct exchange of their electrons.[39] The strength of this interaction depends upon the transfer integral, which decreases exponentially with increasing separation between the cations. Direct exchange between M(1) and M(2) provides the opportunity for overlap on either side of the same M(1) t_{2g} orbital and is predicted to be ferromagnetic. The intercation distance (2.91 Å) is considerably greater than in the β-phase (2.67 Å), where ferromagnetic double exchange between the equivalent sites produces much greater conductivity and an average value for the magnetic moment corresponding to $Fe^{2.5+}$. Direct exchange between M(1) sites is also possible between the t_{2g} orbitals projecting through the shared edges, but this distance is prohibitively large (3.22 Å). As the observed moments for M(1) and M(2) are significantly different, direct double exchange, if present, must be weak.

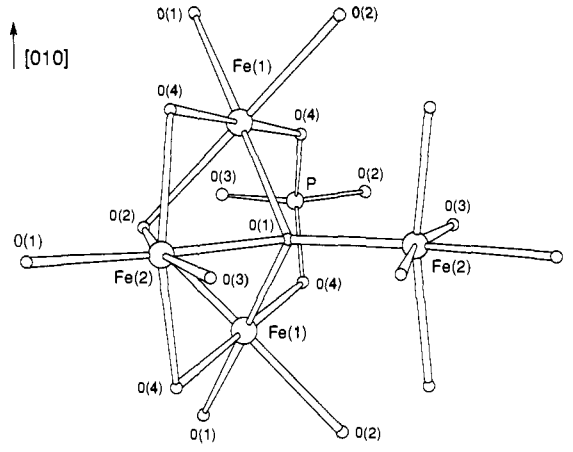

Figure 6. Refined crystal structure of α-Fe_2PO_5 showing possible superexchange pathways (see text).

(ii) Cation–Anion–Cation Superexchange Interactions. Stronger interactions between M(1) sites within a chain are expected between their anion-directed e_g orbitals through the p σ orbitals of the oxygens O(1) and O(2) that share the common edge between the octahedra. M(1)–O(1)–M(1) (2 × 2.044 Å, 103.3°) offers a stronger ferromagnetic exchange pathway than M(1)–O(2)–M(1) (2 × 2.233 Å, 91.9°) due to the shorter distances and hence greater orbital overlap. Ferromagnetic superexchange between M(1) and M(2) sites within a chain may operate via the O(1), O(2), and O(4) anions, with the latter providing the greatest opportunity for orbital overlap (M(1)–O(4)–M(2), 2.111 Å, 2.008 Å, 89.9°). Antiferromagnetic interactions between the chains of ferromagnetically aligned octahedra must exist to maintain the overall antiferromagnetism of the structure. Connections between the chains are available through the shared oxygen O(1) or via the bridging phosphate group O(4)–P–O(4). Weak Fe–O–P–O–Fe superexchange between octahedra occurs in $KBaFe_2(PO_4)_3$[40] between 4.2 and 3.9 K, and stronger interactions are observed in $Na_3Fe_2(PO_4)_3$,[3] $NaFeP_2O_7$,[4] and $Fe_3(PO_4)_2$[7] with Néel temperatures of 29, 47, and 44 K, respectively. However, as the magnetic ordering temperature of α-Fe_2PO_5 is considerably higher (250 K), it would seem more likely that the shorter superexchange pathways through the O(1) oxygen will dominate.

The M(1)–O(1)–M(2) pathway between the chains (2.044 Å, 1.879 Å, 87.1°) involves the shortest M–O bonds within each octahedron and appears to offer the strongest possibilities for exchange. The bonds contract significantly on lowering the temperature from 300 to 12 K, with O(1)–M(2) decreasing by 0.020 (4) Å and the two symmetric M(1)–O(1) bonds decreasing by 0.009 (2) Å. In contradiction to the observed ordering, ferromagnetic interactions are predicted for 90° d^6–d^5 superexchange, indicating that the other pathway between chains from M(2)–O(1)–M(2) (2.181 Å, 1.879 Å, 133.6°) must be responsible for

(36) Clementi, E.; Roetti, C. *At. Data Nucl. Data Tables* **1974**, *14*, 177.
(37) Brown, P. J.; Matthewman, J. C. Rutherford Appleton Research Laboratories Report, RAL-87-010, 1987.
(38) Cox, D. E. *IEEE Trans. Magn.* **1972**, Vol. MAG-8, No. 1, 161.
(39) Goodenough, J. B. *Magnetism and the Chemical Bond*; Wiley: New York, 1963; pp 180–190.
(40) Battle, P. D.; Cheetham, A. K.; Harrison, W. T. A.; Long, G. L. *J. Solid State Chem.* **1986**, *62*, 16.

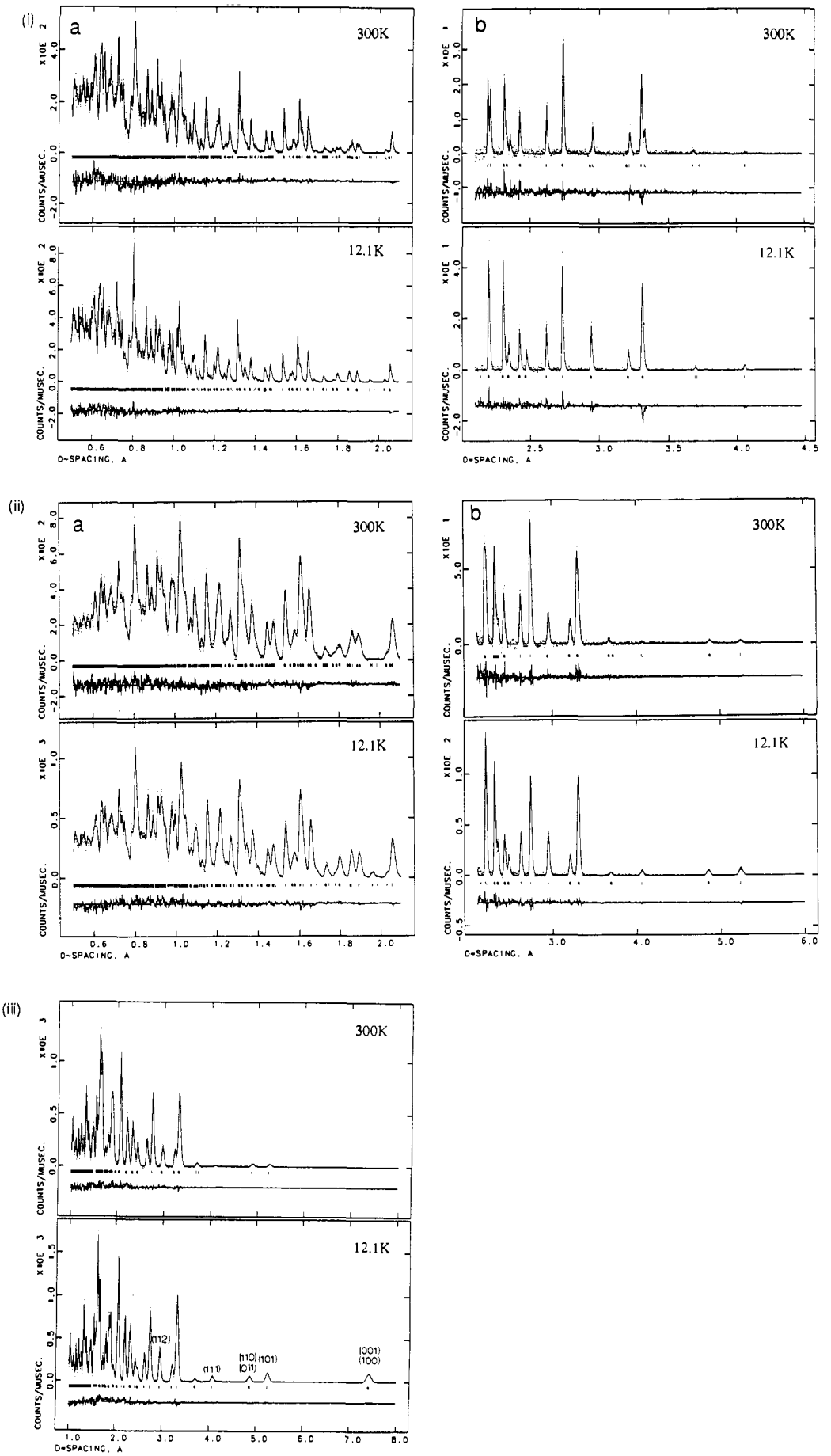

Figure 7. Observed (dots), calculated (solid line), and difference profiles of time-of-flight neutron data at 300 and 12.1 K measured at detector angles (i) 153°, (ii) 90°, and (iii) 40°. The first two data sets have been split into (a) small and (b) long *d* space regions to give appropriate scales. The reflection positions are shown by marker bars. The strongest magnetic peaks have been labeled.

Table IV. Bond Distances, Valences, and Angles Calculated from 300 K Time-of-Flight Neutron Powder Data

distance (Å)		s_i	angle (deg)	
M(1)–O(1), (×2)	2.053 (1)	0.423 (2)	O(1)–M(1)–O(4)[a]	98.62 (6)
M(1)–O(2), (×2)	2.231 (1)	0.261 (1)	O(1)–M(1)–O(2)	108.52 (5)
M(1)–O(4),[a] (×2)	2.118 (1)	0.354 (1)	O(2)–M(1)–O(4)[a]	100.19 (6)
$\sum s_i$(M(1))		2.077 (3)		
M(2)–O(1)[b]	1.899 (2)	0.684 (4)	O(1)–M(2)–O(1)[b]	165.81 (7)
M(2)–O(1)	2.149 (2)	0.348 (2)	O(2)–M(2)–O(3)	167.11 (10)
M(2)–O(2)	2.210 (2)	0.295 (2)	O(4)–M(2)–O(4)[a]	160.22 (9)
M(2)–O(3)	1.905 (2)	0.674 (4)	O(1)–M(2)–O(3)	96.94 (9)
M(2)–O(4),[a] (×2)	2.018 (1)	0.497 (1)	O(1)[a]–M(2)–O(4)	97.11 (5)
$\sum s_i$(M(2))		2.997 (7)	O(2)–M(2)–O(4)	82.49 (4)
P–O(2)	1.557 (3)	1.176 (9)	O(2)–P–O(3)[a]	110.94 (17)
P–O(3)	1.517 (3)	1.311 (10)	O(2)–P–O(4)	108.54 (12)
P–O(4),[b,c] (×2)	1.535 (2)	1.249 (5)	O(3)[a]–P–O(4)[c]	111.15 (12)
$\sum s_i$(P)		4.985 (16)	O(4)[a]–P–O(4)[c]	106.36 (16)
$\sum s_i$(O(1))		−1.878 (5)		
$\sum s_i$(O(2))		−1.994 (10)		
$\sum s_i$(O(3))		−1.985 (11)		
$\sum s_i$(O(4))		−2.101 (5)		

[a] Symmetry transformation: x, $^1/_2 - y$, z, or its operator related by the center of symmetry. [b] Symmetry transformation: $^1/_2 - x$, $^1/_2 + y$, $^1/_2 + z$, or its operator related by the center of symmetry. [c] Symmetry transformation: $^1/_2 - x$, $-y$, $^1/_2 + z$, or its operator related by the center of symmetry.

the overall antiferromagnetism of the structure. As both 90° and 180° superexchange models predict antiferromagnetic ordering between d^5 cations, the intermediate angle observed for this pathway is still consistent with the theory.[39]

The observed and calculated profiles for the time-of-flight neutron data are shown in Figure 7. Bond strengths (s_i) and the valences of various sites ($\sum s_i$) were calculated using the program STRUMO.[41] Table IV lists the bond distances, valences, and angles calculated from the 300 K neutron data. The excellent agreement between expected and calculated valence for the two metal sites supports the assignment of the M(1) site to Fe^{2+} and M(2) to Fe^{3+}.

Conclusions

The valence distribution in α-Fe_2PO_5 has been investigated by resonant X-ray diffraction and magnetic neutron scattering, and the findings have been compared with the results of bond strength calculations. The values of the anomalous scattering corrections determined for the two different crystallographic sites are consistent with the presence of Fe^{2+} on M(1) and Fe^{3+} on M(2), but the agreement with the theoretical values, which do not currently take into account effects such as the influence of bonding on near-edge fine structure, is only qualitative. Thus, on the basis of these measurements alone, we could not exclude the possibility that the valence ordering is only partial. The magnetic moments obtained from the low-temperature, magnetic neutron diffraction study are also in qualitative agreement with the same valence distribution, though again there is uncertainty as to what values of magnetic moments should be expected for Fe^{2+} and Fe^{3+} in this particular structure. By contrast, the valence bond method, which is an indirect and empirical probe of valence ordering, indicates unambiguously that complete ordering indeed takes place. Due to uncertainties such as the magnitude of the orbital contribution to the magnetic moment of Fe^{2+}, there seems little prospect that the magnetic scattering technique will be able to furnish a quantitative picture of valence distributions in Fe^{2+}/Fe^{3+} systems in the near future, but there is reason to hope that further experimental and theoretical work in the anomalous scattering area may well lead to more quantitative findings by the X-ray method. Such studies will require diffraction data at several wavelengths in the vicinity of the absorption edge.

Acknowledgment. The authors thank Dr. A. P. Wilkinson for helpful discussions and assistance with data collection, the Association of Commonwealth Universities for the provision of a Commonwealth Scholarship to J.K.W., Shell (Amsterdam) for their financial support, and the SERC for the use of the synchrotron beam line. Work at Brookhaven was supported by the Division of Materials Science, U.S. Department of Energy, under Contract No. DE-AC02-76CH00016.

Registry No. Fe_2PO_5, 81208-51-7.

Supplementary Material Available: A table of instrumental parameters from X-ray powder diffraction data sets and a table of refined instrumental parameters from time-of-flight neutron data (2 pages). Ordering information is given on any current masthead page.

(41) Brown, I. D.; Altermatt, D.; et al. *STRUMO, A modelling program for inorganic structures*; Version 1991.3.12; Institute for Materials Research, McMaster University: Hamilton, Ontario L8S 4MI, Canada.